Circuit Modeling of Carrier–Photon Dynamics in Composite-Resonator Vertical-Cavity Lasers

Bhavin J. Shastri, *Student Member, IEEE*, Chen Chen, *Member, IEEE*, Kent D. Choquette, *Fellow, IEEE*, and David V. Plant, *Fellow, IEEE*

***Abstract*— We present a circuit model for composite-resonator vertical-cavity lasers (CRVCLs) based on the standard rate equations. This model is compatible with general-purpose circuit analysis program (SPICE), and it can accurately produce the dc and modulation characteristics of the CRVCL, which is verified by comparing the calculated results with the measured experimental data. In addition, using this model we verify that CRVCL has unique abilities to engineer its modulation characteristics by varying cavity asymmetries as well as to produce multilevel amplitude modulation, both of which are consistent with our previous experimental results. We also discuss some advantages and limitations of this model.**

***Index Terms*— Circuit modeling, circuit simulation, coupled cavity, equivalent circuits, optoelectronics, semiconductor lasers, SPICE, vertical-cavity surface-emitting lasers.**

I. Introduction

THE vertical-cavity surface-emitting laser (VCSEL) has become a dominant laser source for short-haul optical communications owing to its ability for low-cost high-volume manufacture, low power consumption, and high-speed modulation. Meanwhile, the VCSEL consisting of two optically coupled cavities, which is known as the composite-resonator vertical-cavity laser (CRVCL) [1], has enabled the use of modulation techniques beyond the conventional direct modulation and has demonstrated the potential to improve VCSEL bandwidth [2]–[5]. Compared to the VCSEL, the CRVCL can offer additional functionalities such as multilevel signal generation, microwave signal mixing and short pulse generation [5], [6]. These functionalities have become possible because the CRVCL has the flexibility to modulate its laser output by using either one or both of its optical cavities, and by exploiting other modulation techniques such as eletroabsorption and push-pull modulation [7], [8]. These functionalities have also made the CRVCL attractive to emerging applications such as high-performance computers, data centers and access networks, where integrated functionalities are demanded to minimize the form factor and energy consumption of future optical systems.

Apart from the experimental demonstrations of the CRVCL characteristics and functionalities in the previous work [1]–[8], device modeling of the CRVCL has been studied extensively by analytically or numerically solving the laser rate equations [1], [5], [9]–[11]. Mathematically, the rate equations for the CRVCL are more involved than those for the conventional VCSEL, due to the complex nature of the photon-carrier dynamics in the coupled cavities. For example, the photons within one optical mode can simultaneously interact with the gain medium and the charge carriers in both cavities; and the CRVCL also has the possibility to lase on two different longitudinal wavelengths. Thus in order to accurately account for these complex photon-carrier interactions, it is often inevitable that we must resort to the computationally intensive numerical solution of the rate equations.

Alternatively, one can transform the CRVCL rate equations into a circuit model, which can then be solved using circuit analysis techniques. This method has been used widely to model the quantum well laser and VCSEL [12]–[14]. Not only does this method enable to expedite the computation of the rate equations, but also it can facilitate a computer-aid design (CAD) and ease the analysis of an integrated optoelectronic system. Therefore, in this paper we describe the circuit-level modeling of the CRVCL for the first time, to the best of our knowledge. This paper provides a mathematical description of the transformation from the CRVCL rate equations to its circuit model. Using the SPICE circuit analysis, the circuit model can produce both the dc and modulation properties of the CRVCL, which are then verified with the measured characteristics of the CRVCL. For the high-speed modulation of the CRVCL, our present circuit model focuses on the direct modulation approach, that is, the light output of the CRVCL is modulated through either or both of its cavities. We verify that the asymmetries between the coupled cavities play a significant role in determining the CRVCL modulation response, which is consistent with our observation from the previous experimental results [5]. This circuit model coupled

Manuscript received June 1, 2011; revised August 16, 2011; accepted September 11, 2011. Date of current version October 28, 2011. The work of B. J. Shastri was supported in part by the Natural Sciences and Engineering Research Council of Canada through an Alexander Graham Bell Canada Graduate Scholarship and by McGill University through a Lorne Trottier Engineering Graduate Fellowship and McGill Engineering Doctoral Award.

B. J. Shastri was with the Photonic Systems Group, Department of Electrical and Computer Engineering, McGill University, Montreal, QC H3A 2A7, Canada. He is now with the Department of Electrical Engineering, Lightwave Communications Laboratory, Princeton University, Princeton, NJ 08544 USA (e-mail: shastri@ieee.org).

C. Chen was with the Photonic Systems Group, Department of Electrical and Computer Engineering, McGill University, Montreal, QC H3A 2A7, Canada. He is now with Ciena Corporation, Ottawa, ON K2H 8E9, Canada (e-mail: chenchen@ciena.com).

K. D. Choquette is with the Department of Electrical and Computer Engineering, University of Illinois at Urbana-Champaign, Urbana, IL 61801 USA (e-mail: choquett@illinois.edu).

D. V. Plant is with the Department of Electrical and Computer Engineering, Photonic Systems Group, McGill University, Montreal, QC H3A 2A7, Canada (e-mail: david.plant@mcgill.ca).

Color versions of one or more of the figures in this paper are available online at http://ieeexplore.ieee.org.

Digital Object Identifier 10.1109/JQE.2011.2170403

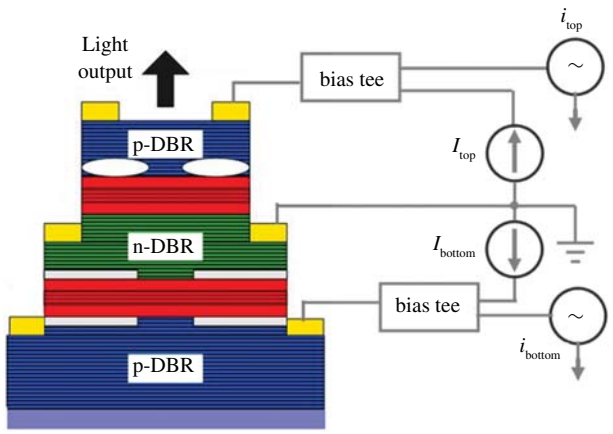

Fig. 1. Schematic of the CRVCL device structure.

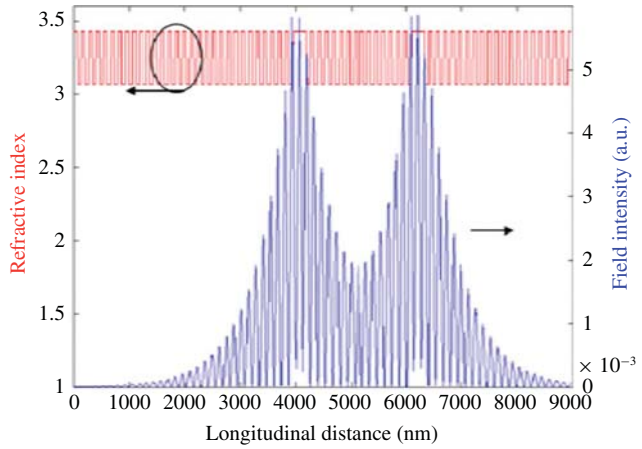

Fig. 2. Calculated refractive index and normalized optical field intensity for the short-wavelength longitudinal mode along the growth direction of a CRVCL, when the top and bottom cavities have the same optical path length.

with the analysis will also provide input for engineering future CRVCLs with unique characteristics.

Following this introduction, the rest of the paper is organized as follows: In Section III, we present the rate equation model of the CRVCL. The circuit-level implementation to model the CRVCL is detailed in Section IV. Section V is devoted to the presentation, analysis, and comparison of the simulation results to measured data. Finally, the paper is summarized and concluded in Section VI.

II. CRVCL Device Structure

Unlike a conventional VCSEL, the photon population within a CRVCL is coupled to the carrier populations in both cavities simultaneously. The laser output of the CRVCL can be varied by applying electrical modulation to either or both of the coupled cavities. Fig. 1 illustrates the device structure of the CRVCL used in this study. The CRVCL is fabricated from an epitaxial wafer consisting of a monolithic bottom p-type distributed Bragg reflector (DBR) with 35 periods, a middle n-type DBR with 12.5 periods, and an upper p-type DBR with 22 periods. The middle DBR mirrors separate two optical cavities, each of which contains five GaAs–$Al_{0.2}Ga_{0.8}As$ quantum well nominally lasing at 850 nm. The two laser cavities are optically coupled but electrically independent. A ground-signal-signal-ground (GSSG) coplanar contact is used, in order to facilitate high-speed signaling into both optical cavities. The details about the CRVCL fabrication procedure can be found in [15].

It is interesting to note that the asymmetries between the coupled cavities of the CRVCL play a role in determining its modulation response. These asymmetries can be exploited to engineer the CRVCL modulation response, and ultimately, to achieve a higher modulation bandwidth than that of a conventional VCSEL. In practice, the asymmetries between the coupled cavities can be varied by the CRVCL epitaxial structure and/or the dc operation points. Here, we show that cavity detuning, which governs the longitudinal mode distribution within a CRVCL, can be used to produce the cavity asymmetry and to engineer the modulation response.

The cavity detuning is a unique property of the coupled-cavity structure, which allows a longitudinal optical mode to preferentially distribute toward one cavity or the other. Fig. 2 depicts the calculated optical field distribution in a CRVCL for the shorter wavelength longitudinal mode. The percentage of the optical field overlapping with the top and bottom cavity is denoted as ξ_1 and ξ_2, respectively. If the two CRVCL cavities have the same optical path length, the longitudinal modes distribute equally between the two cavities, and thus ξ_1 and ξ_2 are equal to 50%. Note that the total photon density in a CRVCL is constant, that is, $\xi_1 + \xi_2 = 1$. The two cavities can also be detuned from each other, such that one cavity can have a longer optical path length than the other. The optical field of the shorter wavelength longitudinal mode shifts toward the laser facet (substrate), when the top cavity has a shorter (longer) optical path length than the bottom cavity [8].

III. CRVCL Rate Equation Model

The coupled rate equations for the carrier and photon densities for CRVCLs, assuming only one longitudinal and one transverse optical mode is lasing, are given by [2], [11], [16]

$$\frac{dN_1}{dt} = \frac{\eta_{i1} I_1}{q V_{act1}} - \frac{N_1}{\tau_1} - v_{g1} \frac{g(N_1)}{\phi_1(S)} \xi_1 S \tag{1}$$

$$\frac{dN_2}{dt} = \frac{\eta_{i2} I_2}{q V_{act2}} - \frac{N_2}{\tau_2} - v_{g2} \frac{g(N_2)}{\phi_2(S)} \xi_2 S \tag{2}$$

$$\frac{dS}{dt} = -\frac{S}{\tau_p} + \Gamma_1 v_{g1} \frac{g(N_1)}{\phi_1(S)} \xi_1 S + \Gamma_2 v_{g2} \frac{g(N_2)}{\phi_2(S)} \xi_2 S + \frac{\beta_1 N_1}{\tau_1} + \frac{\beta_2 N_2}{\tau_2}. \tag{3}$$

Equations (1) and (2) relate the rate of change in the active region's carrier concentration N_k to the injection current I_k, the carrier recombination rate, and the stimulated-emission rate. Note that the top and bottom cavities are represented by the subscript $k = 1$ and 2, respectively. Equation (3) relates the rate of change in photon density S that is common to both cavities, to photon loss, the rate of coupled recombination into the lasing mode, and the stimulated-emission rate. Additionally, η_{ik} is the current-injection efficiency, V_{actk} is the active region volume, q is the electron charge, τ_k is the rate of carrier

recombination, v_{gk} is the group velocity of the optical mode in the lasing medium, ξ_k is the percentage of the optical standing wave overlapping with the respective cavity, τ_p is the photon lifetime, Γ_k is the optical confinement factor, and β_k is the spontaneous-emission coupling factor.

In the above equations, the stimulated-emission rate includes a carrier-dependent gain term $g(N_k)$ as well as the gain-saturation term $\phi_k^{-1}(S)$. The carrier-dependent gain term is defined as [17]

$$g\,(N_k) = g_{k0} \ln\left[\frac{N_k + N_{fk}}{N_{\mathrm{tr}k} + N_{fk}}\right] \tag{4}$$

where g_{k0} is the empirical gain coefficient, $N_{\mathrm{tr}k}$ is the optical transparency carrier density, and N_{fk} is a shift to force the natural logarithm to be finite at $N_k = 0$ such that the gain equals the unpumped absorption. Furthermore, the gain-saturation term is given by [18]

$$\phi_k^{-1}(S) = \frac{1}{1 + \varepsilon_k \Gamma_k S} \tag{5}$$

where ε_k is the phenomenological gain-compression factor. Note that $\phi_k^{-1}(S)$ is positive for all $S \geq 0$, and can be approximated by the linear form when $S \ll (1/\varepsilon_k)\Gamma_k$.

Moving forward, the total laser output power from the coupled cavities can be written as

$$P_{\mathrm{out}} = P_{\mathrm{out}1} + P_{\mathrm{out}2} \tag{6}$$

where $P_{\mathrm{out}k}$ is the output power from the respective cavities given as

$$\frac{\xi_k S}{P_{\mathrm{out}k}} = \frac{\lambda \tau_p}{\eta_c V_{\mathrm{act}k} hc} = \vartheta_k \tag{7}$$

where λ is the lasing wavelength, η_c is the output power coupling coefficent, h is Planck's constant, and c is the speed of light in a vacuum. Consequently, the CRVCL output power can then be expressed as

$$\frac{S}{P_{\mathrm{out}}} = \left[\frac{\xi_1}{\vartheta_1} + \frac{\xi_2}{\vartheta_2}\right]^{-1} = \psi. \tag{8}$$

IV. CRVCL Equivalent Circuit Model

Operating point (steady-state) analysis of the CRVCL described by the rate equations (1)–(3) and the output power (8), leads to four solutions for a given set of injection currents $\{I_1, I_2\}$ to the respective cavities. After some rearrangement of (1)–(3) under the steady-state condition $d/dt = 0$, we lead to the following set of nonlinear dc equations:

$$\begin{aligned} H_1(S, N_1) &= \frac{N_1}{\tau_1} + \Gamma_1 v_{g1} \frac{g\,(N_1)}{\phi_1\,(S)} \xi_1 S - \frac{\eta_{i1} I_1}{q V_{\mathrm{act}1}} \\ &= 0 \end{aligned} \tag{9}$$

$$\begin{aligned} H_2(S, N_2) &= \frac{N_2}{\tau_2} + \Gamma_2 v_{g2} \frac{g\,(N_2)}{\phi_2\,(S)} \xi_2 S - \frac{\eta_{i2} I_2}{q V_{\mathrm{act}2}} \\ &= 0 \end{aligned} \tag{10}$$

$$\begin{aligned} H_3(S, N_1, N_2) &= \frac{S}{\tau_p} + \frac{N_1}{\tau_1}\,[1 - \beta_1] + \frac{N_2}{\tau_2}\,[1 - \beta_2] \\ &\quad - \frac{\eta_{i1} I_1}{q V_{\mathrm{act}1}} - \frac{\eta_{i2} I_2}{q V_{\mathrm{act}2}} \\ &= 0. \end{aligned} \tag{11}$$

Note that (11) is obtained by combining (1) and (2) in order to eliminate the stimulated-emission term. Equations (9)–(11) implicitly define functions $N_1 = f_1(S)$, $N_2 = f_2(S)$, and $(N_1, N_2) = f_3(S)$, as follows:

$$H_1(S, N_1) = 0 \Rightarrow N_1 = f_1(S) \tag{12}$$

$$H_2(S, N_2) = 0 \Rightarrow N_2 = f_2(S) \tag{13}$$

$$H_3(S, N_1, N_2) = 0 \Rightarrow (N_1, N_2) = f_3(S). \tag{14}$$

Equations (12)–(14) map out the solutions of (9)–(11), respectively. The intersection points of these three functions are the valid solutions to the dc rate equations. In addition to the correct nonnegative solution regime, in which the solutions for the carrier densities N_1 and N_2, and photon density S, are all nonnegative when $I_1 \geq 0$ and $I_2 \geq 0$, there are also a negative-power and a high-power regime. Based on the proof in [19], it can be shown that regardless of whether or not there are solution regimes with negative values for N_1, N_2, or S, there is always a *unique* nonnegative solution to (9)–(11) when $I_1 \geq 0$ and $I_2 \geq 0$. Consequently, in order to eliminate the nonphysical solutions—negative-power and a high-power regime—and improve the convergence properties of the model during simulation, we transform the carrier population density in the respective cavities N_k and the laser output power P_{out} via the following pair of transformations, respectively [20]:

$$N_k = N_{k0} \exp\left(\frac{q V_k}{nkT}\right) \tag{15}$$

$$P_{\mathrm{out}} = (V_m + \delta)^2 \tag{16}$$

where, N_{k0} is the equilibrium carrier density, V_k is the voltage across the respective cavities of the laser, n is a diode ideality factor (typically set to two for GaAs–AlGaAs devices [21]), V_m is a new variable for parameterizing P_{out}, δ is a small arbitrary constant set to 10^{-60}, k is Boltzmann's constant, and T is the temperature of the CRVCL.

Fig. 3 shows the circuit-level implementation to model the CRVCL. This equivalent circuit is obtained through suitable manipulations of the rate equations (1)–(3), the output power (8), and the pair of variable transformations (15) and (16). More specifically, we model the carrier's dynamics dN_k/dt, by substituting the transformations (15) and (16), and the output power (8), into the rate equations (1) and (2). After applying appropriate manipulations, we obtain

$$\begin{aligned} &\frac{q N_{k0}}{nkT} \exp\left(\frac{q V_k}{nkT}\right) \frac{dV_k}{dt} \\ &\quad = \frac{\eta_{ik} I_k}{q V_{\mathrm{act}k}} - \frac{N_{k0}}{\tau_k}\left[\exp\left(\frac{q V_k}{nkT}\right) - 1\right] - \frac{N_{k0}}{\tau_k} \\ &\qquad - \psi \xi_k v_{gk} \frac{g\,(N_k)}{\phi_k\big(\psi (V_m + \delta)^2\big)}\,(V_m + \delta)^2\,. \end{aligned} \tag{17}$$

With some additional rearrangement, (17) can be written in terms of the respective cavity currents as

$$I_k = I_k^{T1} + I_k^{T2} + B_k^N \tag{18}$$

where

$$I_k^{T1} = I_k^{D1} + I_k^{C1} \tag{19}$$

$$I_k^{T2} = I_k^{D2} + I_k^{C2} \tag{20}$$

$$I_k^{D1} = \frac{qN_{k0}V_{\text{act}k}}{2\eta_{ik}\tau_k}\left[\exp\left(\frac{qV_k}{nkT}\right) - 1\right] \tag{21}$$

$$I_k^{D2} = \frac{qN_{k0}V_{\text{act}k}}{2\eta_{ik}\tau_k}\left[\exp\left(\frac{qV_k}{nkT}\right) - 1 + \frac{2q\tau_k}{nkT}\exp\left(\frac{qV_k}{nkT}\right)\frac{dV_k}{dt}\right] \tag{22}$$

$$I_k^{C1} = I_k^{C2} = \frac{qN_{k0}V_{\text{act}k}}{2\eta_{ik}\tau_k} \tag{23}$$

$$B_k^N = \frac{\lambda\tau_p q v_{gk}\Gamma_k}{\eta_{ik}\eta_c hc}\frac{g\left(\Theta_k I_k^{T1}\right)}{\phi_k\left(\psi\cdot(V_m+\delta)^2\right)}(V_m+\delta)^2 \times\left[1+\left(\frac{\xi_1 V_{\text{act1}}}{\xi_2 V_{\text{act2}}}\right)^{(-1)^k}\right]^{-1} \tag{24}$$

with

$$\Theta_k = \frac{2\eta_{ik}\tau_k}{qV_{\text{act}k}} \quad \text{and} \quad N_k = \Theta_k I_k^{T1}. \tag{25}$$

Similarly, to model the photon dynamics dS/dt, we substitute the transformations (15) and (16) and the output power (8), into the rate equations (3). After applying appropriate manipulations, we obtain

$$2(V_m+\delta)\frac{dV_m}{dt} = -\frac{(V_m+\delta)^2}{\tau_p} + \frac{\beta_1 N_1}{\psi\tau_1} + \frac{\beta_2 N_2}{\psi\tau_2} + \left\{\Gamma_1 v_{g1}\xi_1\frac{g(N_1)}{\phi_1\left(\psi(V_m+\delta)^2\right)} + \Gamma_2 v_{g2}\xi_2\frac{g(N_2)}{\phi_2\left(\psi(V_m+\delta)^2\right)}\right\}(V_m+\delta)^2. \tag{26}$$

With some additional rearrangements and the definition of suitable circuit elements, (26) can be rewritten as

$$C_{ph}\frac{dV_m}{dt} + \frac{V_m}{R_{ph}} = B_1^S + B_2^S + G_1^S + G_2^S \tag{27}$$

where

$$G_k^S = \frac{2\eta_{ik}\eta_c hc\beta_k\xi_k}{\lambda q(V_m+\delta)}\left[1+\left(\frac{\xi_1 V_{\text{act1}}}{\xi_2 V_{\text{act2}}}\right)^{(-1)^k}\right] I_k^{T1} \tag{28}$$

$$B_k^S = \tau_p\Gamma_k v_{gk}\xi_k\frac{g\left(\Theta_k I_k^{T1}\right)}{\phi_k\left(\psi\cdot(V_m+\delta)^2\right)}(V_m+\delta) - \delta \tag{29}$$

with

$$C_{\text{ph}} = 2\tau_p \quad \text{and} \quad R_{\text{ph}} = 1\Omega. \tag{30}$$

Finally, B_{pf} transforms the node voltage V_m, into the output power P_{out}, by

$$P_{\text{out}} = B_{\text{pf}} = (V_m+\delta)^2. \tag{31}$$

These equations can be mapped directly into an equivalent CRVCL circuit model as shown in Fig. 3, where p_k and n_k are the electrical (+ve and −ve) terminals of the top and bottom cavity, and p_{f} is the terminal whose node voltage models the output power. Diodes D_k^1 and D_k^2, and current sources I_k^{C1} and I_k^{C2}, model the linear recombination and charge storage in both the cavities. The nonlinear dependent current sources B_k^N, model the effect of stimulated emission on the carrier densities in both the cavities. R_{ph} and C_{ph} help model the time-variation of the photon density under the effect of spontaneous and stimulated emission, which are accounted for by the nonlinear dependent current sources G_k^S and B_k^S, respectively. Finally, the nonlinear voltage source B_{pf}, produces the CRVCL optical output power in the form of a voltage.

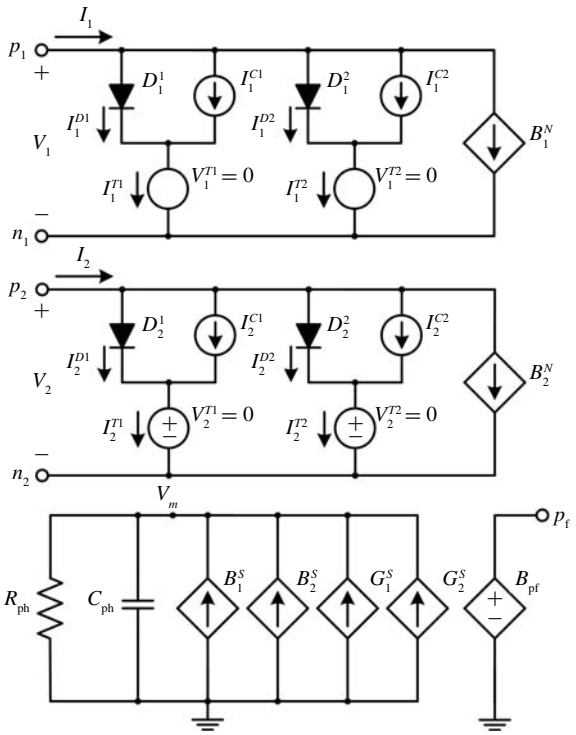

Fig. 3. Circuit-level implementation to model the CRVCL.

For our analysis, unless otherwise mentioned, we consider a typical CRVCL with material and geometrical parameters as given in Table I [5], [8], [15], [17]. We note that the bottom cavity active region volume is twice the top cavity active region volume. In addition, Fig. 4 depicts the simulation setup used to test the CRVCL equivalent circuit model in Fig. 3. In the simulation setup, the dc current sources I_k^{DC}, provide the bias conditions for the top and bottom cavity, whereas the ac current sources i_k^{AC}, provide the small-signals required to modulate the respective cavities. The dc and ac signals are combined via standard bias-T networks formed with the ac coupling capacitances C_k, and the dc coupling inductances L_k. To model the RC parasitics for a CRVCL tested in an experimental setup, we include: (1) the differential series resistance for the cavities as R_{sk}; and (2) the parallel capacitance between the contact pads of the CRVCL and the junction capacitance of the top cavity as C_{pk}. The values of R_{sk} can be obtained from the measured voltage-current (VI) characteristics of the CRVCL [15], whereas the parasitic capacitances are extracted by fitting the measured small-signal

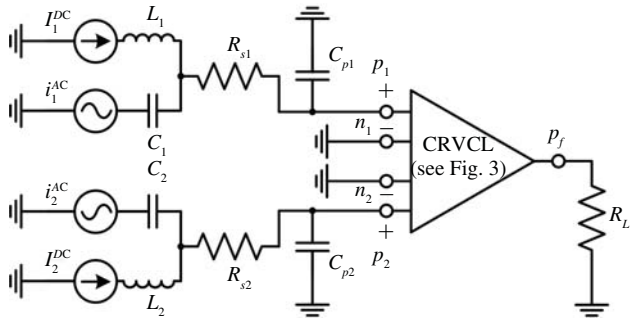

Fig. 4. Circuit setup to simulate the CRVCL equivalent circuit model.

TABLE I
CRVCL DEVICE PARAMETERS USED IN EQUIVALENT CIRCUIT MODEL [5], [8], [15], [17]

Parameter	Description	Value
η_1, η_2	Current-injection efficiency	0.86
λ	Lasing wavelength	850 nm
V_{act1}	Top cavity active region volume	1.2×10^{-18} m^3
V_{act2}	Bottom cavity active region volume	2.4×10^{-18} m^3
Γ_1, Γ_2	Optical confinement factor	0.055
v_{g1}, v_{g2}	Lasing medium group velocity	$3/3.5\times10^{10}$ cm/s
ξ_1, ξ_2	Optical standing wave overlap factor	0.5
τ_1, τ_2	Carrier lifetime	2.6 ns
τ_p	Photon lifetime	2.5 ps
g_{10}, g_{20}	Gain fitting coefficient	3000 cm^{-1}
g_1', g_2'	Differential gain	1×10^{-16} cm^{-2}
S_0	Photon density	4×10^{16} cm^{-3}
N_{tr1}, N_{tr2}	Optical transparency carrier density	2×10^{18} cm^{-3}
N_{f1}, N_{f2}	Unpumped gain fitting parameter	1×10^{18} cm^{-3}
$\varepsilon_1, \varepsilon_2$	Phenomenological gain-saturation term	1.1×10^{-17} cm^3
β_1, β_2	Spontaneous emission coupling factor	0.001
η_c	Output-power coupling coefficient	0.4
N_{10}, N_{20}	Equilibrium carrier density	7.86×10^{9} cm^{-3}

TABLE II
CRVCL SIMULATION SETUP CIRCUIT PARAMETERS

Element	Description	Value
C_1, C_2	AC coupling capacitance	1 F
L_1, L_2	DC coupling inductance	1 H
R_{s1}	Top cavity series resistance	590 Ω
R_{s2}	Bottom cavity series resistance	205 Ω
C_{p1}	Top cavity parasitic resistance	14.4 pF
C_{p2}	Bottom cavity parasitic resistance	4 pF
R_L	Load resistance	1 GΩ

modulation responses. Lastly, the dummy load R_L, enables the measurement of output power from the CRVCL circuit model. The simulation setup circuit parameters are given in Table II.

V. RESULTS AND DISCUSSION

A. Steady-State Analysis

Figs. 5(a) and 5(b) show the simulated CRVCL circuit model and the experimental light-current (LI) characteristics of the top and bottom cavities, for different dc currents in the bottom and top cavity, respectively. The CRVCL light output

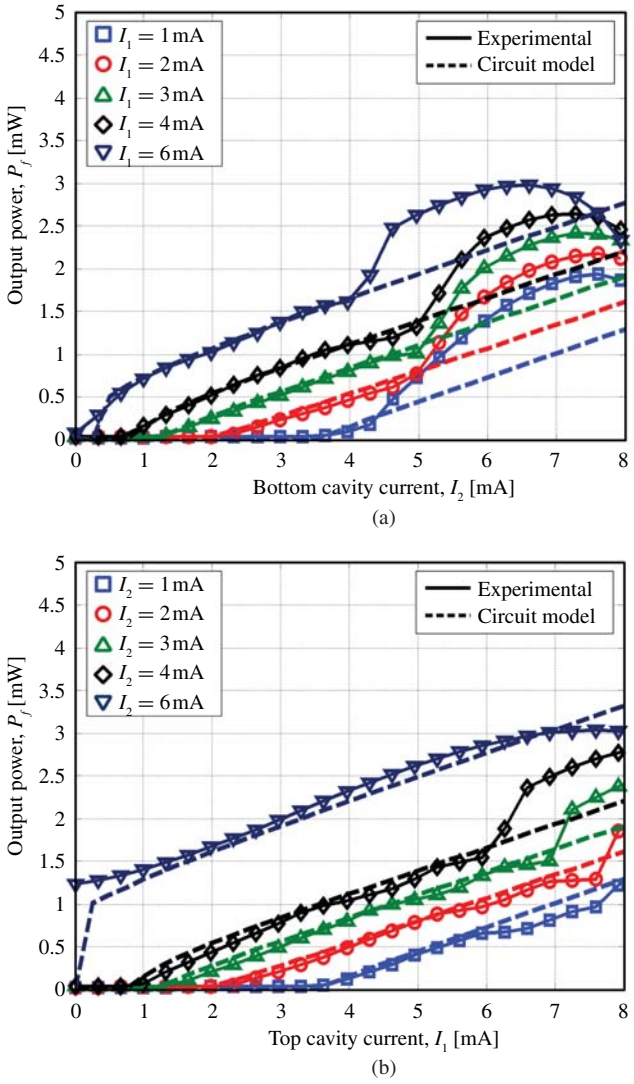

Fig. 5. Light-current characteristics of the (a) top cavity with different bottom cavity currents and (b) bottom cavity with different top cavity currents.

increases and threshold current decreases, as a larger dc current is applied to the top or bottom cavity resulting in increasing laser gain, as expected from prior CRVCL study [2]. The simulation results are in close agreement with the experimental data to the first-order; that is, in terms of threshold current and slope efficiency. However, the second-order characteristic of the CRVCL is not accounted for in the equivalent circuit model. This is illustrated by the kinks in the experimental curves for high dc currents which represent the transition from the shorter-wavelength to the longer-wavelength longitudinal mode. Because the two longitudinal modes of a CRVCL often experience different modal gain at given a dc current in the top and bottom cavity, the optical power distribution between the longitudinal modes varies with the dc current [22]. However, it is also possible for the CRVCL to lase on only one longitudinal mode by engineering spectral alignment between the cavity modes and material gain. Also note that the thermal effect is not considered in the circuit model, thus LI derivation due to thermal roll-over cannot be accounted.

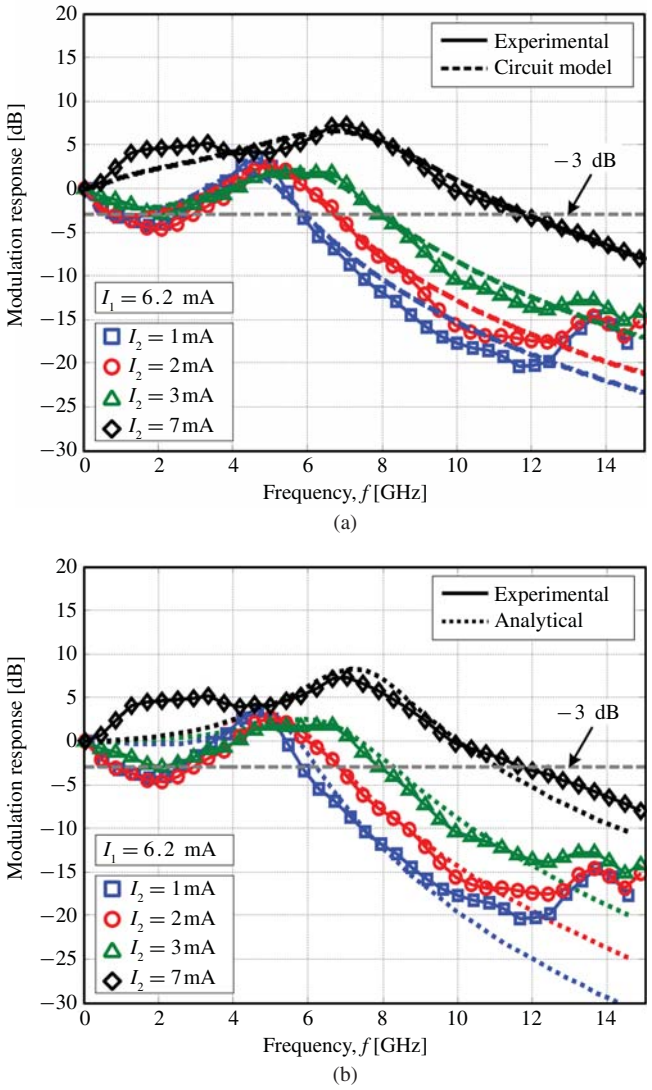

Fig. 6. Small-signal modulation response with different bottom cavity currents. Experimental results compared to (a) circuit model simulation and (b) analytical model.

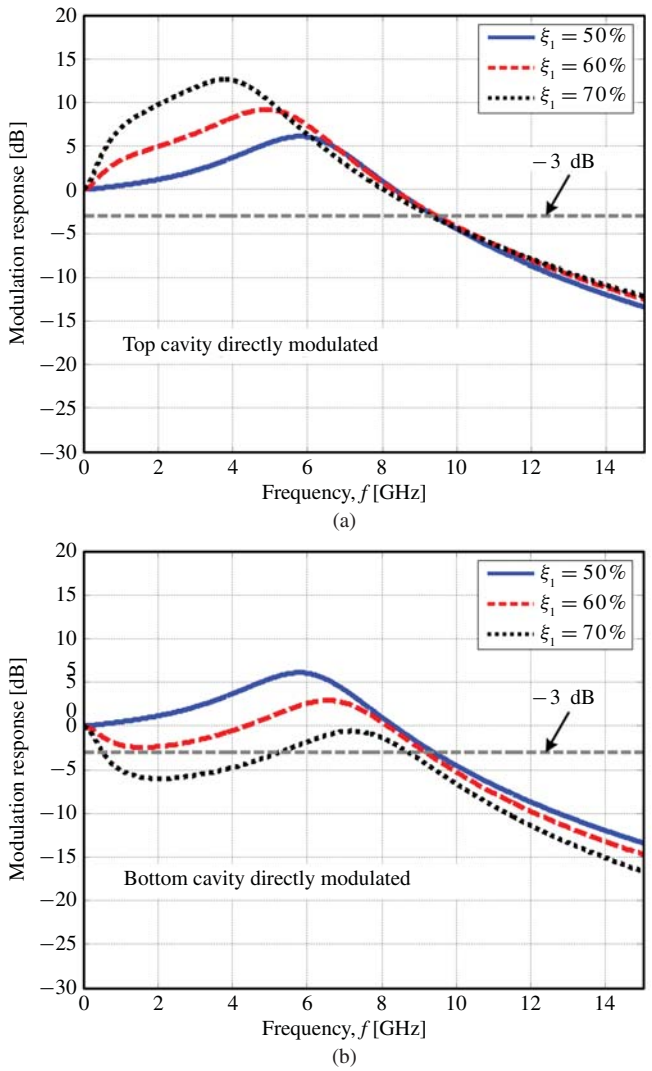

Fig. 7. Small-signal modulation response as a function of the fraction of the longitudinal optical field in the top cavity, when the (a) top and (b) bottom cavity is under direct modulation. A fixed photon density is assumed.

B. Small-Signal Analysis

1) Modulation Response Characteristics: Fig. 6(b) illustrates the simulated CRVCL circuit model and the experimental small-signal response of the CRVCL when the direct modulation is applied only to the top cavity. The modulation response is measured with different dc currents in the bottom cavity, while the dc current in the top cavity is fixed at 6.2 mA. For all the bottom dc currents used in Fig. 6(b) only one longitudinal mode is lasing dominantly, so that these experimental conditions are agreed with the single mode assumption of the rate equation except that higher-order transverse modes can still exist. Specifically, the shorter-wavelength longitudinal mode dominates when the bottom currents are 1 mA, 2 mA and 3 mA, while the longer-wavelength longitudinal mode dominates for the bottom current of 7 mA.

It can be observed that the relaxation oscillation (RO) frequency pushes to a higher frequency with the increasing bottom cavity current, which is expected due to the increasing photon density in the CRVCL. The maximum modulation bandwidth is 12 GHz, which is limited by the photon number (or the optical power) of the CRVCL. The simulation results are in close agreement with the experimental data.

The CRVCL rate equations (1)–(3) were solved analytically in prior work to study the laser dynamics under direct modulation [2], [8]. Before moving forward, we compare the experimental results with those obtained from this standard analytical model. The direct modulation response through the top and bottom cavity can be expressed as (32) and (34) (shown at the top of the next page), respectively. In these equations, g_k' is the material gain, S_0 is the photon density in a single longitudinal and transverse mode, d_k is the active region thickness, ω is the angular modulation frequency, $i = \sqrt{-1}$, $s(\omega)$ and $j_k(\omega)$ are the small-signal photon density and current density, respectively. The values of these parameters are listed in Table I. The measured modulation responses can be fitted analytically using (32) as shown in Fig. 6(a). While the curves compare reasonably well to the experimental results

$$\left|\frac{s(\omega)}{j_1(\omega)}\right| = \left|\frac{\Gamma_1 v_1 g_1' S_0/qd_1}{\omega^2 + i\omega(1/\tau_1 + v_1 g_1' \xi_1 S_0) - v_1^2 \Gamma_1 \xi_1 g_{10} g_1' S_0 - v_2^2 \Gamma_2 \xi_2 g_{20} g_2' S_0 \gamma}\right| \tag{32}$$

$$\gamma = \frac{i\omega - (1/\tau_1 + v_1 g_1' \xi_1 S_0)}{i\omega - (1/\tau_2 + v_2 g_2' \xi_2 S_0)}. \tag{33}$$

$$\left|\frac{s(\omega)}{j_2(\omega)}\right| = \left|\frac{\Gamma_2 v_2 g_2' S_0/qd_2}{\omega^2 + i\omega(1/\tau_2 + v_2 g_2' \xi_2 S_0) - v_2^2 \Gamma_2 \xi_2 g_{20} g_2' S_0 - v_1^2 \Gamma_1 \xi_1 g_{10} g_1' S_0/\gamma}\right| \tag{34}$$

above the RO frequency including the RC bandwidth, they do not compare well for frequencies below the RO frequency. This is not the case with the proposed circuit model where the results are comparable across all frequencies. It should be noted that the analytical model solves the rate equations algebraically obtaining a closed-form expression, whereas the circuit model solves the rate equations numerically by accounting for the interdependence between laser parameters. The proposed circuit model provides an improvement over the existing analytical model.

2) Cavity Detuning Characteristics: Fig. 7(a) shows the simulated CRVCL circuit model modulation response as a function of the percentage of the optical longitudinal mode overlapping with the top cavity (ξ_1), when only the top cavity is under direct modulation. The simulations depicted in Fig. 7(a) only vary (ξ_1) and assume the other cavity parameters are the same for both cavities. Although different optical field distribution may lead to changes in other cavity parameters, such as the gain coefficient and differential gain, the proposed equivalent CRVCL circuit model use these simplified assumptions. It can be observed from Fig. 7(a) that the modulation response has an increasing RO peak and greater modulation bandwidth as more optical field is confined in the top cavity. On the other hand, Fig. 7(b) shows the CRVCL modulation response as a function of ξ_1, when only the bottom cavity is under direct modulation. Similarly, the modulation response can be engineered by varying the detuning between both cavities. However, it is interesting to observe that the modulation response exhibits the opposite trend as compared to Fig. 7(a).

The case when $\xi_1 = 50\%$ in Figs. 7(a) and 7(b) correspond to the same modulation response, which is also equivalent to the modulation response of a conventional VCSEL with the same photon density. When more optical field is confined in the top cavity, the modulation response becomes more damped (decreasing RO peak) and the modulation bandwidth decreases. Therefore, for a given ξ_1, we can obtain two different modulation responses, depending on which cavity we have chosen to apply direct modulation. For an appropriate ξ_1, the CRVCL would achieve a larger bandwidth than that of a conventional VCSEL with the same photon density. This is consistent with the observation obtained in prior work [2]. The dependence of the modulation responses on ξ_1 in Fig. 7 can be explained by analyzing the poles and zeros of (32) and (34) [15].

C. Transient Analysis—Multilevel Amplitude Modulation

Multilevel amplitude modulation, also known as M-level pulse-amplitude modulation (PAM-M), is widely used in digital communications to achieve higher data throughput and spectra efficiency than the conventional binary on-off keying (OOK) modulation [23]. More specifically, PAM-M encodes M bits in each transmission period such that aggregate data rate increases by a factor of M compared to OOK modulation. In light of this, PAM-4 signaling of a VCSEL has been explored in prior work, as an alternative approach to achieve higher speed digital modulation [24]. PAM-4 signaling can achieve better link performance than OOK modulation, especially at the data rates for which the VCSEL is bandwidth-limited [24]. PAM-4 signaling also has the ability to mitigate frequency-dependent attenuation and fiber dispersion, and thus lower the link budget [25]. In addition, PAM-4 signaling offers an advantage in VCSEL reliability, because it requires lower modulation bandwidth and thus smaller current density for a given data rate as compared to OOK modulation. However, PAM-4 signaling also increases the complexity of the design and implementation of VCSEL driver circuits, preventing the widespread system-level evaluation of VCSEL-based PAM-4 signaling.

The CRVCL offers advantages for PAM-4 signaling. As demonstrated in [5], the total modulation response of a CRVCL under direct modulation is the superposition of the modulation responses from the top and bottom cavities. This unique property enables the CRVCL to produce a PAM-4 optical signal by combining two binary amplitude modulation electrical signals in the coupled cavities. Furthermore, the CRVCL does not require complex driver circuits to produce a PAM-4 signal. Instead, each CRVCL cavity can be driven by binary signaling circuits that are much simpler to implement and commercially available. CRVCL also has the ability to produce different PAM-4 waveforms by adjusting the relative amplitude between the modulation signals for both cavities.

Fig. 8(a) illustrates the output optical signal at 5 Gb/s when only the top cavity is modulated with a 5 GHz square wave ($1010\cdots$) electrical signal varying between 4–8 mA, and the bottom cavity is biased at 4 mA. Similarly, Fig. 8(b) is the output optical power of the CRVCL at 10 Gb/s in response to a 10 GHz square wave electrical pulse input to the bottom cavity, varying between 5–7 mA with the top cavity biased at 4 mA. Fig. 8(c) shows the optical output signal consisting of four amplitude levels as a result of simultaneously applying

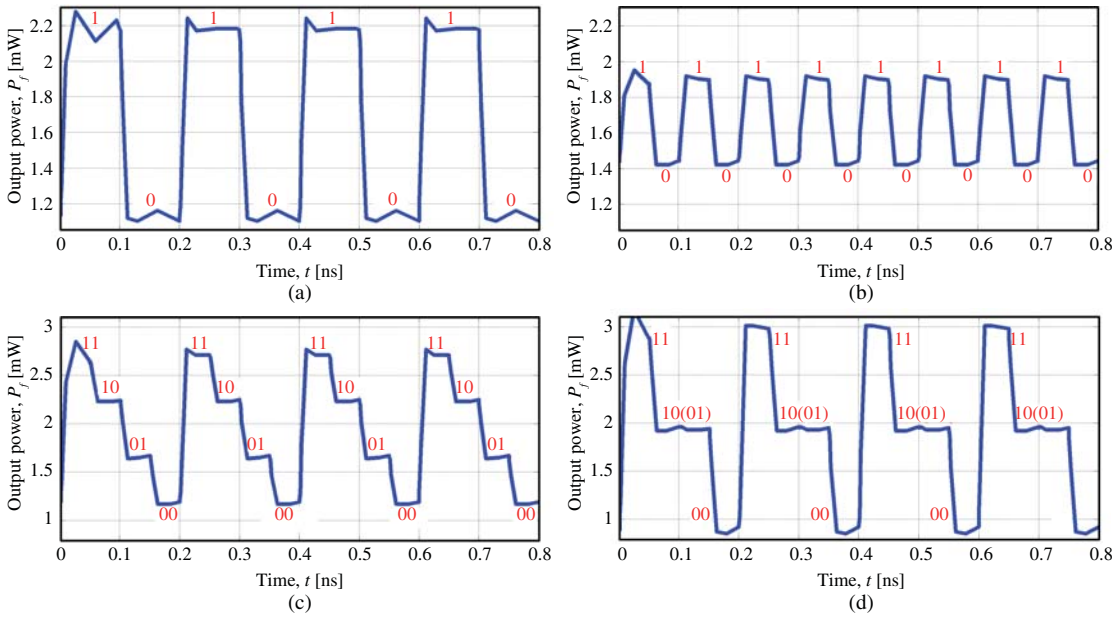

Fig. 8. Circuit modeling of optical output signal when only the (a) top cavity and (b) bottom cavity is under direct modulation. Optical output signal when (c) 6-dB and (d) 0-dB attenuation is applied to the bottom cavity relative to the top cavity, given that both cavities are under direct modulation simultaneously.

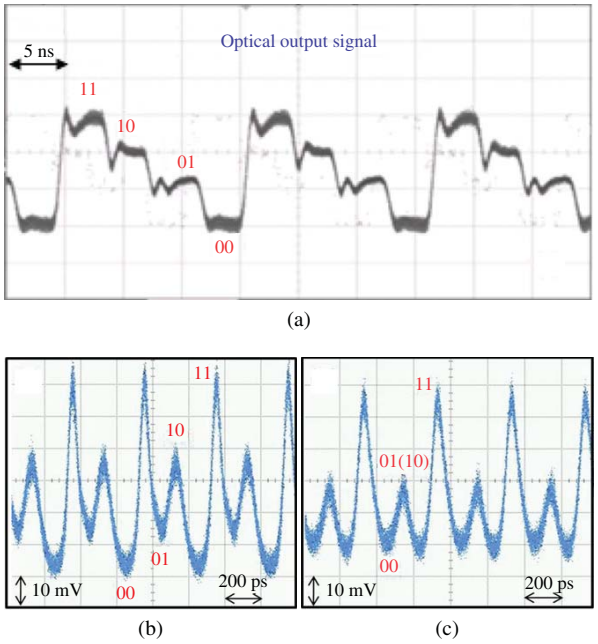

Fig. 9. Experimental optical output signal when both cavities are under direct modulation simultaneously. (a) 125 Mb/s PAM-4 signaling. (b) 10 Gb/s PAM-4 signaling. (c) 10 Gb/s PAM-3 signaling.

direct modulation to the top and bottom cavity; that is, a result of adding the individual modulation responses from the both cavities. The highest (or lowest) amplitude level denoted as 11 (or 00) is achieved when both input signals are switched high (or low). The intermediate level 10 and 01 corresponds to the individual modulation response from the bottom and top cavity, respectively. It should be noted that in Fig. 8(c), the bottom cavity is modulated with a signal attenuated by 6 dB relative to the modulating signal applied to the top cavity. The relative amplitude for the intermediate levels 10 and 01 vary as the amplitude of the modulation response from the top or bottom cavity increases or decreases with respect to each other. As shown in Fig. 8(d), when the modulating signals to the top and bottom cavity are at the same level, the optical output signal has only three levels with the two intermediate amplitude levels, 10 and 01 coinciding, producing a three-level PAM signaling. The simulated CRVCL circuit model results are consistent with our previous experimental results. Fig. 9 shows the experimental optical output signal when both cavities are under direct modulation simultaneously. More specifically, Fig. 9(a) is obtained for PAM-4 signaling at 125 Mb/s in [26] whereas Figs. 9(b) and 9(c) show PAM-4 and PAM-3 signaling at 10 Gb/s [6].

VI. Conclusion

In this paper we have proposed an equivalent circuit model for the CRVCL. We describe the mathematical transformation that links the CRVCL rate equations to the circuit equations, which are then solved using SPICE analysis to produce the dc and modulation properties of the CRVCL. Furthermore, we show that the calculated CRVCL characteristics from the circuit model can achieve a close agreement with the measured experimental data in term of threshold current, slope efficiency and small-signal modulation response, thank to its self-consistency that accounts for the interdependence between laser parameters. However, the circuit model does not account for some higher-order dc and modulation effects, such as the kinks in the LI curves due to longitudinal mode switching and thermal roll-over, because the model is derived based on the assumption that the CRVCL lases on single longitudinal and transverse optical mode. Therefore, the circuit model needs to be expanded in the future to account for those effects. In the case of considering the second longitudinal

mode, another photon equation needs to be added and the electrical carrier equations (1) and (2) need to be modified so that the carriers are consumed by two simulated emission processes; we also need to consider the cross terms such as the cross gain compression and phase detuning of two longitudinal modes. Due to the additional interdependence between photons and carriers interactions, the rate equations can be only solved using numerical methods such as the Runge-Kutta method [15]. In this paper, we show that by mapping the CRCVL rate equations into a circuit model, SPICE analysis can be used as an efficient and accurate implementation of numerical calculations. And we believe that this circuit approach would also provide a smooth upgrade when more complex higher-order CRVCL effects are incorporated in the future. Nevertheless, the current circuit model will still be useful when a predominant single longitudinal mode is desired for applications such as push-pull modulation [8]. This single longitudinal mode condition can be achieved by setting a proper cavity detuning and/or gain/cavity spectral alignment.

In addition, we have verified that using the proposed circuit model, the asymmetries between the coupled cavities can be used to engineer the CRCVL modulation response. We also confirm the CRVCL's unique ability to produce multilevel amplitude modulation. Both observations are consistent with our previous experimental results. This circuit model and its analysis will provide a useful design toolbox to engineer the unique characteristics of CRVCL in the future.

REFERENCES

[1] A. J. Fischer, K. D. Choquette, W. W. Chow, H. Q. Hou, and K. M. Geib, "Coupled-resonator vertical-cavity laser diode," *Appl. Phys. Lett.*, vol. 75, no. 19, pp. 3020–3022, Nov. 1999.

[2] D. M. Grasso, D. K. Serkland, G. M. Peake, K. M. Geib, and K. D. Choquette, "Direct modulation characteristics of composite resonator vertical-cavity lasers," *IEEE J. Quantum Electron.*, vol. 42, no. 12, pp. 1248–1254, Dec. 2006.

[3] V. A. Shchukin, N. N. Ledentsov, J. A. Lott, H. Quast, F. Hopfer, L. Y. Karachinsky, M. Kuntz, P. Moser, A. Mutig, A. Strittmatter, V. P. Kalosha, and D. Bimberg, "Ultrahigh-speed electro-optically modulated VCSELs: Modeling and experimental results," *Proc. SPIE*, vol. 6889, no. 1, p. 68890H, Jan. 2008.

[4] J. V. Eisden, M. Yakimov, V. Tokranov, M. Varanasi, E. M. Mohammed, I. Young, and S. Ortyabrsky, "Optical decoupled loss modulation in a duo-cavity VCSEL," *IEEE Photon. Technol. Lett.*, vol. 20, no. 1, pp. 42–44, Jan. 2008.

[5] C. Chen and K. D. Choquette, "Analog and digital functionalities of composite-resonator vertical-cavity lasers," *J. Lightw. Technol.*, vol. 28, no. 7, pp. 1003–1010, Apr. 2010.

[6] C. Chen, Z. Tian, K. D. Choquette, and D. V. Plant, "Reconfigurable functionalities of coupled-cavity VCSELs using digital modulation," in *Proc. Opt. Fiber Commun. Conf.*, 2010, no. OMQ4, pp. 1–3.

[7] C. Chen, P. O. Leisher, D. M. Grasso, C. Long, and K. D. Choquette, "High-speed electroabsorption modulation of composite-resonator vertical-cavity lasers," *IET Optoelectron.*, vol. 3, no. 2, pp. 93–99, Apr. 2009.

[8] C. Chen, K. L. Johnson, M. Hibbs-Brenner, and K. D. Choquette, "Pushpull modulation of a composite-resonator vertical-cavity laser," *IEEE J. Quantum Electron.*, vol. 46, no. 4, pp. 438–446, Apr. 2010.

[9] G. P. Agrawal, "Coupled-cavity semiconductor lasers under current modulation: Small-signal analysis," *IEEE J. Quantum Electron.*, vol. 21, no. 3, pp. 255–263, Mar. 1985.

[10] W. W. Chow, "Composite resonator mode description of coupled lasers," *IEEE J. Quantum Electron.*, vol. 22, no. 8, pp. 1174–1183, Aug. 1986.

[11] V. Badilita, J.-F. Carlin, M. Ilegems, and K. Panajotov, "Rate-equation model for coupled-cavity surface-emitting lasers," *IEEE J. Quantum Electron.*, vol. 40, no. 12, pp. 1646–1656, Dec. 2004.

[12] B. P. C. Tsou and D. L. Pulfrey, "A versatile SPICE model for quantum well lasers," *IEEE J. Quantum Electron.*, vol. 33, no. 2, pp. 246–254, Feb. 1997.

[13] M. R. Salehi and B. Cabon, "Circuit modeling of quantum-well lasers for optolelectronic integrated circuits (ICs) including physical effect of deep-level trap," *IEEE J. Quantum Electron.*, vol. 38, no. 11, pp. 1510–1514, Nov. 2002.

[14] P. V. Mena, J. J. Morikuni, S.-M. Kang, A. V. Harton, and K. W. Wyatte, "A comprehensive circuit-level model of vertical-cavity surface-emitting lasers," *J. Lightw. Technol.*, vol. 17, no. 12, pp. 2612–2632, Dec. 1999.

[15] C. Chen, "Coupled cavity surface emitting lasers: Modulation concepts, performance and applications," Ph.D. dissertation, Dept. Electr. Comput. Eng., Univ. Illinois, Urbana-Champaign, Urbana, Apr. 2009.

[16] S. L. Chuang, *Physics Optoelectronics Devices*. New York: Wiley, 1995.

[17] L. A. Coldren and S. W. Corzine, *Diode Lasers Photonic Integrated Circuits*. New York: Wiley, 1995.

[18] D. J. Channin, "Effect of gain saturation on injection laser switching," *J. Appl. Phys.*, vol. 50, no. 6, pp. 3858–3860, Jun. 1979.

[19] P. V. Mena, S.-M. Kang, and T. A. Detemple, "Rate-equation based laser model with a single solution regime," *J. Lightw. Technol.*, vol. 15, no. 4, pp. 717–730, Apr. 1997.

[20] S. A. Javro and S. M. Kang, "Transforming Tucker's linearized laser rate equations to a form that has a single solution regime," *J. Lightw. Technol.*, vol. 13, no. 9, pp. 1899–1904, Sep. 1995.

[21] R. S. Tucker and D. J. Pope, "Circuit modeling of the effect of diffusion on damping in a narrow-stripe semiconductor laser," *IEEE J. Quantum Electron.*, vol. 19, no. 7, pp. 1179–1183, Jul. 1983.

[22] A. C. Lehman and K. D. Choquette, "Threshold gain temperature dependence of composite resonator vertical-cavity lasers," *IEEE J. Quantum Electron.*, vol. 11, no. 5, pp. 962–967, Sep.–Oct. 2005.

[23] J. G. Proakis and M. Saleshi, *Communication Systems Engineering*. Englewood Cliffs, NJ: Prentice-Hall, 2002.

[24] J. E. Cunningham, D. Beckman, X. Zheng, D. Huang, T. Sze, and A. V. Krishnamoorthy, "PAM-4 signaling over VCSELs with 0.13 μm CMOS chip technology," *Opt. Exp.*, vol. 14, no. 25, pp. 12028–12038, Dec. 2006.

[25] S. Walkin and J. Conradi, "Multilevel signaling for increasing the reach of 10 Gb/s lightwave systems," *J. Lightw. Technol.*, vol. 17, no. 11, pp. 2235–2248, Nov. 1999.

[26] C. Chen and K. D. Choquette, "Multilevel amplitude modulation using a composite-resonator vertical-cavity laser," *IEEE Photon. Technol. Lett.*, vol. 21, no. 15, pp. 1030–1032, Aug. 2000.

Bhavin J. Shastri (S'03) received the B.Eng. (with distinction honors) and M.Eng. degrees in electrical engineering from McGill University, Montreal, QC, Canada, in 2005 and 2007, respectively. He is currently pursuing the Ph.D. degree in electrical engineering with the Photonic Systems Group, McGill University.

His current research interests include high-speed burst-mode clock, data recovery circuits, and optoelectronic circuits.

Mr. Shastri is a Student Member of the IEEE Photonics Society, the Optical Society of America (OSA), and the International Society for Optics and Photonics (SPIE). He was the President and Co-Founder of the McGill OSA Student Chapter. He is the recipient of a prestigious IEEE Photonics Society Graduate Student Fellowship in 2011. He was also awarded a SPIE Scholarship in Optics and Photonics in 2011. He is a Lorne Trottier Engineering Graduate Fellow and a winner of the prestigious Alexander Graham Bell Canada Graduate Scholarship from the National Sciences and Engineering Research Council of Canada. He was the recipient of the Best Student Paper Award (2nd place) from the IEEE International Midwest Symposium on Circuits and Systems in 2010, the co-recipient of the Silver Leaf Certificate for the Best Student Paper from the IEEE Microsystems and Nanoelectronics Research Conference in 2008, and the recipient of the IEEE Photonics Society Travel Grant in 2007. He was the winner of the IEEE Computer Society Lance Stafford Larson Outstanding Student Award in 2004 and the IEEE Canada Life Member Award for the Best Student Paper in 2003.

Chen Chen (M'10) received the B.S., M.S., and Ph.D. degrees in electrical and computer engineering from the University of Illinois at Urbana-Champaign, Urbana, in 2004, 2006, and 2009, respectively.

He is currently with Ciena Corporation, Ottawa, ON, Canada. From 2009 to 2011, he was a Post-Doctoral Fellow with the Photonics System Group, McGill University, Montreal, QC, Canada. He is the author or co-author of more than 50 journal and conference publications. His current research interests include semiconductor lasers and optoelectronics devices, optical interconnects, coherent optical transmission, and optical networking.

Kent D. Choquette (M'97–F'03) received the B.S. degree in engineering physics and applied mathematics from the University of Colorado-Boulder, Boulder, and the M.S. and Ph.D. degrees in materials science from the University of Wisconsin-Madison, Madison.

He held a post-doctoral appointment at AT&T Bell Laboratories, Murray Hill, NJ, and then joined Sandia National Laboratories, Albuquerque, NM. In 2000, he joined the Electrical and Computer Engineering Department, University of Illinois at Urbana-Champaign, Urbana. His Photonic Device Research Group is centered around the design, fabrication, characterization, and application of vertical cavity surface-emitting lasers, photonic crystal light sources, nanofabrication technologies, and hybrid integration techniques. He has authored more than 200 technical publications and three book chapters, and has presented numerous invited talks and tutorials.

Dr. Choquette has served as an Associate Editor of the IEEE JOURNAL OF QUANTUM ELECTRONICS, the IEEE PHOTONICS TECHNOLOGY LETTERS, and the IEEE/OSA *Journal of Lightwave Technology*, as well as a Guest Editor of the IEEE JOURNAL OF SELECTED TOPICS IN QUANTUM ELECTRONICS. He was awarded the IEEE Laser and Electro-Optics Society Engineering Achievement Award in 2008. He is a fellow of the Optical Society of America and the International Society for Optics and Photonics.

David V. Plant (S'85–M'89–SM'05–F'07) received the Ph.D. degree in electrical engineering from Brown University, Providence, RI, in 1989.

He was a Research Engineer with the Department of Electrical and Computer Engineering, University of California, Los Angeles, from 1989 to 1993. He has been a Professor and member of the Photonic Systems Group, Department of Electrical and Computer Engineering, McGill University, Montreal, QC, Canada, since 1993, and the Chair of the department since 2006. He is the Director and Principal Investigator with the Center for Advanced Systems and Technologies Communications, McGill University. From 2000 to 2001, he left from McGill University to become the Director of the Optical Integration, Accelight Networks, Pittsburgh, PA. His current research interests include optoelectronic-very large-scale integration, analog circuits for communication, electro-optic switching devices, and optical network design including optical code division multiple access, radio-over-fiber, and agile packet switched networks.

Dr. Plant has received five teaching awards from McGill University, including most recently the Principal's Prize for Teaching Excellence in 2006. He is a James McGill Professor and an IEEE LEOS Distinguished Lecturer. He was the recipient of the R. A. Fessenden Medal and the Outstanding Educator Award both from IEEE Canada, and received a NSERC Synergy Award for Innovation. He is a member of Sigma Xi and a fellow of the Optical Society of America.